ALP contribution to the strong *CP* problem

V. Enguita,[1,*] B. Gavela,[1,†] B. Grinstein,[2,‡] and P. Quílez[2,§]

[1]*Departamento de Física Teórica, Universidad Autónoma de Madrid, and IFT UAM-CSIC, Madrid, Spain*
[2]*Department of Physics, University of California, San Diego, California, USA*

(Received 3 April 2024; accepted 30 May 2024; published 23 July 2024)

We compute the one-loop contribution to the $\bar{\theta}$ parameter of an faxionlike particle (ALP) with *CP*-odd derivative couplings. Its contribution to the neutron electric dipole moment is shown to be orders of magnitude larger than that stemming from the one-loop ALP contributions to the up- and down-quark electric and chromoelectric dipole moments. This strongly improves existing bounds on ALP-fermion *CP*-odd interactions and also sets limits on previously unconstrained couplings. The case of a general singlet scalar is analyzed as well. In addition, we explore how the bounds are modified in the presence of a Peccei-Quinn symmetry.

DOI: 10.1103/PhysRevD.110.015024

I. INTRODUCTION

Axionlike particles (ALPs) are singlet pseudo-Goldstone bosons (pGBs) that emerge as a consequence of the spontaneous breaking of a global symmetry. They are motivated by a variety of scenarios that aim to solve some of the shortcomings of the Standard Model of particle physics (SM). This includes scenarios that solve the strong *CP* problem [1–4], theories with extra space-time dimensions [5–8], some dynamical flavor theories [9–12], dark matter models [13–15], scenarios that explore a dynamical origin for Majorana neutrino masses [16] and string theory models [17], among others. Consequently, the study of ALPs is currently under intense investigation, marked by a surge in experimental proposals and robust theoretical endeavors. The most prominent among those pGB candidates is the QCD axion [1–4], which aims to explain the absence of *CP* violation in the strong sector by dynamically relaxing the $\bar{\theta}$ parameter to the *CP* conserving point.

Flavor preserving, low energy *CP*-odd observables are predicted by the SM to be very small, since they are suppressed by a combination of small quark masses and small CKM mixing angles, and first arise at multiloop level in the perturbative expansion. Hence, they are powerful probes of new sources of *CP* violation. Prime among these observables is the electric dipole moment (EDM) of the neutron (nEDM), whose dominant contribution in the SM arises from penguin diagrams involving spectator quarks [18,19] and is estimated to be several orders of magnitude smaller than the current experimental bound [20,21].

In this work, we focus on the case of a generic ALP (i.e., with shift-symmetric couplings to SM fermions). Inspired by the QCD axion, most of the effort in ALP phenomenology has been devoted to study the *CP*-conserving couplings of ALPs to SM particles. However, *CP*-violating ALP signatures are gaining increased interest [22–30].

Indeed, derivative ALP-fermion interactions can have *CP*-odd couplings, and it turns out that they may contribute to quark electric dipole moments (qEDMs) at one loop. These and the resulting contribution to the nEDM have been computed elsewhere [22]. In this work, we compute instead the one-loop contribution to $\bar{\theta}$ of an ALP with *CP*-odd derivative couplings to the SM quarks. We will show that its contribution to the nEDM is parametrically distinct than that of quark electric dipole moments and can be numerically much more important. For completeness, the contribution to $\bar{\theta}$ of a generic scalar is also computed and compared.

II. SETUP: DERIVATIVE FERMIONIC ALP LAGRANGIAN

Let us consider an ALP a, defined as a spin-0 field,[1] singlet of the SM, and described by a Lagrangian invariant

*victor.enguita@uam.es
†belen.gavela@uam.es
‡bgrinstein@ucsd.edu
§pquilez@ucsd.edu

[1]ALPs with an exact shift symmetry are not necessarily pseudoscalars since the allowed *CP*-odd derivative couplings can be as large as the *CP*-conserving ones, preventing us from assigning a definite transformation property of the ALP under *CP*.

under the shift symmetry $a \to a + \text{constant}$,[2] except for a small mass term $m_a \ll f_a$, where f_a is the ALP physics scale. We focus here on effective ALP-fermion interactions up to $\mathcal{O}(1/f_a)$ terms. At scales $\mu \lesssim f_a$, these purely derivative interactions are encoded in the following effective Lagrangian:

$$\begin{aligned}\mathcal{L}_a \supset & \frac{1}{2}\partial_\mu a \partial^\mu a - \frac{1}{2} m_a^2 a^2 + \left(\bar{u}_L \boldsymbol{M}_u u_R + \bar{d}_L \boldsymbol{M}_d d_R + \text{H.c.}\right) \\ & + \bar{\theta}_0 \frac{\alpha_s}{8\pi} G_{\mu\nu}\tilde{G}^{\mu\nu} + \frac{\partial_\mu a}{f_a}\left(\bar{u}_L \gamma^\mu \boldsymbol{C}_Q u_L + \bar{u}_R \gamma^\mu \boldsymbol{C}_{u_R} u_R \right. \\ & \left. + \bar{d}_L \gamma^\mu \boldsymbol{C}_Q d_L + \bar{d}_R \gamma^\mu \boldsymbol{C}_{d_R} d_R\right), \end{aligned} \tag{1}$$

where m_a is the ALP mass, $\boldsymbol{C}_{Q,u_R,d_R}$ are hermitian 3×3 matrices in flavor space and $\boldsymbol{M}_{u,d}$ are the up-type and down-type quark 3×3 mass matrices. Note that the ALP couplings to u_L and to d_L are identical as mandated by the SM electroweak $SU(2)\times U(1)$ gauge invariance. *Because of the hermiticity of the ALP-fermion coefficient matrices, only the flavor off-diagonal ALP-fermion couplings can lead to observable effects of CP violation*. The SM fermion mass terms are also shown in Eq. (1) and taken to be real and diagonal so that the overall phase of the argument of the determinant of the mass matrices is already included in the $\bar{\theta}$ term, where $\bar{\theta}_0 \equiv \bar{\theta}(\mu = \mu_0)|_{\text{tree}}$ and $\mu_0 \equiv f_a$.

Our objective in this work is to compute the leading contribution of the fermionic ALP couplings to $\bar{\theta}$ (and its subsequent impact on the nEDM), which arises at one loop, as we will see next; see Fig. 1.[3] We assume that the ALP mass is larger than the QCD scale, $m_a \gtrsim 1$ GeV. Let us consider an effective field theory (EFT) below the scale $\mu_2 = \min(m_t, m_a)$. The parameters in this EFT are computed by matching at the scale $\mu = \mu_2$ and receive contributions from integrating out both the ALP and the top quark. Let us focus first on the contribution to the phase of the up-quark mass. The details of the computation of the one-loop diagram in Fig. 1 are given in the next section, but let us anticipate that the contribution to $\bar{\theta}$ will turn out to be dominated by the top loop, provided all entries of $\boldsymbol{C}_{Q,u_R,d_R}$ are of the same order, and reads

$$\Delta\bar{\theta}_{\text{ALP}} \simeq \frac{m_t \max(m_a^2, m_t^2)}{16\pi^2 f_a^2 m_u} \text{Im}\left(\boldsymbol{C}_Q^{13}\boldsymbol{C}_{u_R}^{*13}\right). \tag{2}$$

The dependence of this formula on the top mass is highly relevant; e.g., for $m_a < m_t$, it is cubic, a behavior that will be transmitted to the ensuing contribution to the nEDM. This $\bar{\theta}$-induced contribution to the nEDM will be shown to be several orders of magnitude larger than that obtained in Ref. [22] through the contribution to the quark EDMs, as the latter only depends on m_t linearly.

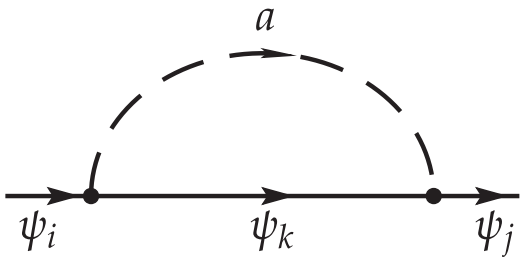

FIG. 1. One-loop corrections to the fermion masses.

The mass dependence in Eq. (2) can be readily understood using the chirality-flip basis (described in Appendix A) instead of the derivative basis in Eq. (1). In the chirality-flip basis, there are two relevant Feynman diagrams to be considered, shown in Fig. 4. In order for the upper diagram in Fig. 4 with an internal top quark to contribute to the $\bar{u}_L u_R$ term, a mass insertion $\propto m_t$ inside the loop provides the required chirality flip. Each vertex contributes a factor of m_t/f_a. Since the loop depends on the renormalization scale only, logarithmically the diagram gives a contribution that scales with m_t and f_a as m_t^3/f_a^2. The loop in the second diagram in Fig. 4 is quadratic in m_a, and the vertex contributes a factor of m_t/f_a^2. So, the contributions of the first and second diagram scale as m_t^3/f_a^2 and $m_t m_a^2/f_a^2$, respectively, and both contain a factor of $\boldsymbol{C}_Q^{13}\boldsymbol{C}_{u_R}^{*13}$. Finally, since we are computing the contribution to the phase of the up-quark mass term, the result is inversely proportional to the absolute value of the quark mass itself, explaining the $1/m_u$ factor in Eq. (2) (see footnote 2).

The result can also be understood in the derivative basis in Eq. (1), in which only the diagram in Fig. 1 contributes, but rather than obtaining the factors of m_t^2 and m_a^2 from the vertices, they arise from the quadratically divergent loop integral. We have verified that both bases give the same results for the explicit computations presented in Sec. III.

It is easy to see as well that the contributions to other CP-violation observables do not scale as $m_t \max(m_t^2, m_a^2)$. Take, for example, the contribution to the quark EDM, d_q, and use again the chirality-flip basis of the Lagrangian. At one loop, it arises exclusively from the diagram in Fig. 3; there is no contribution from the analog of that for the up quark mass from the bottom diagram in Fig. 4 because the photon cannot couple to the neutral axion. The chirality flip and the vertices give a factor of m_t^3/f_a^2, but now dimensional analysis dictates that the loop integral gives an additional factor of $1/m_t^2$ so that $d_q \sim m_t/f_a^2$.

The Lagrangian in Eq. (1) includes all operators that contribute at order $\mathcal{O}(1/f_a^2)$ to $\Delta\bar{\theta}_{\text{ALP}}$ in the derivative basis. There exists a single shift-symmetric operator with mass dimension 5 [33–35] and another one with dimension 6 [36,37], both involving the Higgs. They are not displayed

[2]Anomalous couplings that break the shift invariance are often included in the ALP Lagrangian. In this work, we ignore them.

[3]It has been recently claimed [31,32] that there are small additional contributions that, however, are not included in the standard approach to the calculation of $\bar{\theta}$. The inclusion of this effect would not significantly modify the results of this work.

in Eq. (1) since they are *CP*-even and thus do not contribute to $\Delta\bar{\theta}_{\rm ALP}$. Beyond these, there are *CP*-odd operators with mass dimension 7 and thus $\mathcal{O}(1/f_a^3)$.

It is also worth noting that, since we are assuming $m_a \gtrsim 1$ GeV, including the operator $aG\tilde{G}$ in the Lagrangian would not introduce a dynamical mechanism relaxing $\bar{\theta}$ to zero. That is, it would not amount to promoting the ALP to a QCD axion with a true PQ symmetry (that would require $m_a \to 0$).

III. COMPUTATION OF THE CONTRIBUTION TO $\bar{\theta}$

We perform in this section the one-loop matching of the Lagrangian in Eq. (1) to the following QCD Lagrangian:

$$\begin{aligned}\mathcal{L}_{\rm QCD,CPV} = {}& \bar{\theta}\frac{\alpha_s}{8\pi}G_{\mu\nu}\tilde{G}^{\mu\nu} + \sum_{q=u,d,s}\bar{q}\,m_q q \\ & - \frac{i}{2}\sum_{q=u,d,s}\left[d_q F_{\mu\nu}\bar{q}\sigma^{\mu\nu}\gamma_5 q + g_s\tilde{d}_q G_{\mu\nu}\bar{q}\sigma^{\mu\nu}\gamma_5 q\right] \\ & + \cdots, \end{aligned} \tag{3}$$

where $q = u,\ d,\ s$ denote the three lighter quark fields (up, down and strange quarks), while $d_{u,d,s}$ and $\tilde{d}_{u,d,s}$ stand for their respective qEDMs and chromo-EDMs (cEDMs), and $F_{\mu\nu}$ and $G_{\mu\nu}$ denote the QED and QCD field strength tensors, respectively. Other dimension five operators (such as the Weinberg operator) are left implicit in the ellipsis.

The calculation of $\bar{\theta}$ proceeds in standard effective field theoretical fashion: Starting from the EFT defined in Eq. (1), we run $\bar{\theta}$ from μ_0 to $\mu_1 \approx \max(m_t, m_a)$ and then match θ to θ' defined in EFT′, a new effective theory where the heaviest of the top quark and the ALP have been integrated out. Then run $\bar{\theta}'$ to μ_2 where the lighter of the top quark and the ALP is integrated out and a new θ'' for a new EFT″ is computed. This effective theory is QCD + QED with five flavors of quarks. To perform the calculation, we find the renormalization group equation (RGE) in the EFT, use it to determine the functional form of $\bar{\theta}(\mu)$, giving $\bar{\theta}(\mu_1)$ in terms of the initial (prescribed) value $\bar{\theta}(\mu_0)$, and then compute a threshold correction $\delta\bar{\theta}(\mu_1)$ that fixes the parameter in the EFT′: $\bar{\theta}'(\mu_1) = \bar{\theta}(\mu_1) + \delta\bar{\theta}(\mu_1)$. The process is then repeated in going from EFT′ to EFT″. Finally the RGE is used in the EFT″ to compute $\bar{\theta}''(\mu_{\rm IR})$ where the choice $\mu_{\rm IR} \approx 1$ GeV is common as it is appropriate for computing physical effects such as the nEDM. Henceforth, we drop the double prime in $\bar{\theta}''(\mu_{\rm IR})$. If the ALP is lighter than the b quark, the procedure above is accordingly modified.

At leading order, the ALP contribution to both the running and matching of $\bar{\theta}$ can be obtained using $\bar{\theta} = \theta + \arg\det(\boldsymbol{M}_u^{1\,\rm loop}\boldsymbol{M}_d^{1\,\rm loop})$ by evaluating the ALP-exchange contribution to the one-loop quark mass matrices,

$$\boldsymbol{M}_{u,d}^{1\,\rm loop} = \boldsymbol{M}_{u,d} + \Delta\boldsymbol{M}_{u,d}, \tag{4}$$

where $\boldsymbol{M}_{u,d}$ is the tree level mass, and $\Delta\boldsymbol{M}_{u,d}$ is the correction at one loop; thus,

$$\begin{aligned}\Delta\bar{\theta}_{\rm ALP}(\mu) &= \sum_{q=u,d}\arg\left[\det\left(\boldsymbol{M}_q(1+\boldsymbol{M}_q^{-1}\Delta\boldsymbol{M}_q)\right)\right] \\ &= \sum_{q=u,d}{\rm Im}\left({\rm Tr}\log\left(1+\boldsymbol{M}_q^{-1}\Delta\boldsymbol{M}_q\right)\right) \\ &\simeq \sum_{q=u,d}{\rm ImTr}\left(\boldsymbol{M}_q^{-1}\Delta\boldsymbol{M}_q\right). \end{aligned} \tag{5}$$

Here, as stated earlier, $\boldsymbol{M}_q$ in Eq. (1) is taken to be real, and in the last step, we assumed that the loop correction to the mass is small, $\boldsymbol{M}_{u,d} \gg \Delta\boldsymbol{M}_{u,d}$.[4]

We have computed the one-loop diagram in Fig. 1.[5] The final result using dimensional regularization and the $\overline{\rm MS}$ scheme reads

$$\Delta\bar{\theta}_{\rm ALP}(\mu) \simeq \frac{1}{f_a^2}\sum_{q=u,d}{\rm ImTr}\left[\boldsymbol{M}_q^{-1}\mathbf{C}_Q\boldsymbol{L}\mathbf{C}_{q_R}\right], \tag{6}$$

where $\boldsymbol{L} \equiv {\rm diag}(L_1, L_2, L_3)$, and

$$\begin{aligned}L_k = \frac{m_{q_k}}{16\pi^2}\Bigg[\left(m_a^2 + m_{q_k}^2\right)\left(1+\log\frac{\mu^2}{m_a^2}\right) \\ + \frac{m_{q_k}^4}{m_{q_k}^2 - m_a^2}\log\frac{m_a^2}{m_{q_k}^2}\Bigg], \end{aligned} \tag{7}$$

which explicitly depends on the renormalization scale μ and also includes the finite contributions. In this expression q_k stands for the different type of quarks, i.e., $\{u_1, u_2, u_3\} \equiv \{u, c, t\}$ and $\{d_1, d_2, d_3\} \equiv \{d, s, b\}$. The running of $\bar{\theta}(\mu)$ is determined by the renormalization group equation,

$$\begin{aligned}\frac{d\bar{\theta}}{d\mu} &= \sum_{q=u,d}{\rm Im}\frac{d}{d\mu}\ln\det\boldsymbol{\mathcal{M}}_q = \sum_{q=u,d}{\rm Im}\frac{d}{d\mu}{\rm Tr}\ln\boldsymbol{\mathcal{M}}_q \\ &= \sum_{q=u,d}{\rm ImTr}\left(\boldsymbol{\mathcal{M}}_q^{-1}\frac{d}{d\mu}\boldsymbol{\mathcal{M}}_q\right), \end{aligned} \tag{8}$$

where, to leading order, $\boldsymbol{\mathcal{M}}_{u,d} \equiv \boldsymbol{M}_{u,d}^{1\,\rm loop}$ as given in Eq. (4). Taking into account that the tree-level contribution $\boldsymbol{M}_{u,d}$ is μ independent, it follows that

[4]This approximation breaks down for $m_u \to 0$, which is why the apparent divergence in Eq. (2) in that limit is an artifact.

[5]The renormalization of the kinetic terms does not contribute to $\bar{\theta}$ [38].

$$\mu\frac{d\bar{\theta}}{d\mu} \simeq \sum_{q=u,d} \mathrm{Im}\mathrm{Tr}\left(\boldsymbol{M}_q^{-1}\mu\frac{d}{d\mu}\Delta\boldsymbol{M}_q\right), \tag{9}$$

which, given Eq. (6), leads to

$$\mu\frac{d\bar{\theta}}{d\mu} \simeq \frac{1}{f_a^2}\sum_{q=u,d} \mathrm{Im}\mathrm{Tr}\left[\boldsymbol{M}_q^{-1}\mathbf{C}_Q\boldsymbol{\mathcal{L}}\mathbf{C}_{q_R}\right], \tag{10}$$

where $\boldsymbol{\mathcal{L}} \equiv \mathrm{diag}(\mathcal{L}_1, \mathcal{L}_2, \mathcal{L}_3)$, and

$$\mathcal{L}_k = \frac{m_{q_k}}{8\pi^2}\left(m_a^2 + m_{q_k}^2\right). \tag{11}$$

Neglecting threshold corrections, that is, dropping the matching contribution $\delta\bar{\theta}$ at μ_1 and μ_2, the result of the calculation is

$$\begin{aligned}\bar{\theta}(\mu_{\mathrm{IR}}) \simeq \bar{\theta}_0 + &\sum_{u_i=\{u,c,t\}} \frac{m_{u_k}\left(m_a^2+\hat{m}_{u_k}^2\right)}{16\pi^2 f_a^2 m_{u_i}}\mathrm{Im}\left(\boldsymbol{C}_Q^{ik}\boldsymbol{C}_{u_R}^{*ik}\right)\\ &\times\log\frac{f_a^2}{\max\left(m_a^2, m_{u_k}^2\right)} + \sum_{d_i=\{d,s,b\}}\frac{m_{d_k}\left(m_a^2+\hat{m}_{d_k}^2\right)}{16\pi^2 f_a^2 m_{d_i}}\\ &\times\mathrm{Im}\left(\boldsymbol{C}_Q^{ik}\boldsymbol{C}_{d_R}^{*ik}\right)\log\frac{f_a^2}{\max\left(m_a^2, m_{d_k}^2\right)}.\end{aligned} \tag{12}$$

In this expression, we have included the leading log resummation capturing the effect of QCD, as this is needed to account properly for the μ dependence of the quark masses as explained in Sec. D. This is encoded in the modified masses $\hat{m}_{u_k}$ and $\hat{m}_{d_k}$, as given in Eq. (D4), and implicitly in computing the ratios of masses as $m_{u_k}/m_{u_i} = \bar{m}_{u_k}(\mu)/\bar{m}_{u_i}(\mu)$ or $m_{d_k}/m_{d_i} = \bar{m}_{d_k}(\mu)/\bar{m}_{d_i}(\mu)$, that is, a ratio of running masses at a common renormalization scale μ, cf. Eq. (D3). As discussed after Eq. (2), under the assumption that the combinations $\mathrm{Im}(\boldsymbol{C}_Q^{ik}\boldsymbol{C}_{u,d_R}^{*ik})$ are comparable, the dominant contribution to $\bar{\theta}$ arises from the top loop affecting the phase of the up quark.

Finally, note that Eqs. (6) and (7) produce in addition finite contributions to $\bar{\theta}$, which add to the putative initial value $\bar{\theta}(\mu_0 = f_a)$. Assuming no cancellations, all contributions need to separately comply with the experimental limit $\bar{\theta} \ll 10^{-10}$.[6]

[6]This implies that the initial value of $\bar{\theta}(\mu_0)$ also needs to be small. The bounds on the ALP couplings slightly differ depending on the mechanism that may be responsible for the solution to the strong CP problem at a high scale. If the complete physical $\bar{\theta}$ parameter is set dynamically to be small in the UV, $\bar{\theta}(\mu_0) \ll 10^{-10}$, a nonzero $\bar{\theta}$ parameter is generated solely through the running in Eq. (12). In other solutions [39,40], the finite contributions in Eq. (7) may also be relevant.

IV. NEUTRON EDM AND CEDM IMPACT

The stringent experimental limit on the nEDM, $d_n < 1.8\times10^{-26}\, e\cdot\mathrm{cm}$ (90% C.L.) [20,21], sets important constraints on CP-odd couplings. Furthermore, future experiments are proposed to probe the nEDM at level of $d_n \sim (2\text{–}3)\times10^{-28}\, e\cdot\mathrm{cm}$ [41]. The contribution of the $\bar{\theta}$-parameter to the nEDM, together with that stemming from the up, down and strange qEDMs and cEDMs, $d_{u,d,s}$ and $\tilde{d}_{u,d,s}$, can be estimated[7] to be [42–45]

$$\begin{aligned}d_n = {}&0.6(3)\times10^{-16}\bar{\theta}[e\cdot\mathrm{cm}]\\ &- 0.204(11)d_u + 0.784(28)d_d - 0.0028(17)d_s\\ &- 0.32(15)e\tilde{d}_u + 0.32(15)e\tilde{d}_d - 0.014(7)e\tilde{d}_s.\end{aligned} \tag{13}$$

The coefficients of the qEDMs have been obtained with a ∼5% accuracy by the lattice computation in Ref. [43], whereas the rest of the coefficients, which present larger errors, are taken from QCD sum rule estimates [44–46].[8] In particular, we use the analytical estimates computed in Ref. [46] and update some of the input parameters; see Sec. B for additional details.

Even though nEDM experiments provide at the moment the leading bounds on the CP-odd couplings under discussion, storage ring facilities [47] are expected to provide limits on the proton EDM (pEDM) of the order of $d_p \sim 10^{-29}\, e\cdot\mathrm{cm}$ in the near future [48]. Therefore, the projections of the pEDM bounds are competitive with those for future nEDM measurements. The corresponding dependence of the pEDM reads [49]

$$\begin{aligned}d_p = {}&-1.0(5)\times10^{-16}\bar{\theta}[e\cdot\mathrm{cm}]\\ &+ 0.784(28)d_u - 0.204(11)d_d - 0.0028(17)d_s\\ &- 0.26(14)e\tilde{d}_u + 0.28(14)e\tilde{d}_d + 0.02(1)e\tilde{d}_s.\end{aligned} \tag{14}$$

The estimates for $d_p(\bar{\theta})$ and $d_p(\tilde{d}_{u,d})$ are obtained from the nEDM analytical formulas in Ref. [46] by interchanging $u \leftrightarrow d$; see Sec. B for details. The coefficient of $d_{u,d}$ in the pEDM formula is taken again from the lattice result in Ref. [43]. Experimental limits also follow from measurements of atomic EDMs, such as that of ^{199}Hg [50]. We do not include them in our analysis as they currently give comparable bounds.

Using our final result for the ALP contribution to $\bar{\theta}$ in Eq. (12), and barring cancellations with the $\bar{\theta}_0$ value or other terms, the following constraint on the CP-odd ALP parameters involving the top quark is obtained:

[7]Note that these estimates get modified in the presence of a QCD axion (in addition to the ALP); see Sec. C.

[8]The lattice results in Ref. [43] for the qEDM contributions are well approximated by those obtained with QCD sum rules [46] once the updated values of the chiral condensates are used; see Sec. B.

TABLE I. *ALP case.* Bounds on $|\mathrm{Im}[\boldsymbol{C}_Q^{ij}\boldsymbol{C}_{q_R}^{*ij}]/f_a^2|$ in GeV^{-2} obtained from the $\bar{\theta}$ correction.

$\left\|\mathrm{Im}\left[\boldsymbol{C}_Q^{13}\boldsymbol{C}_{u_R}^{*13}\right]/f_a^2\right\| < \left(\frac{m_t^2}{m_a^2+m_t^2}\right)2\times10^{-17}$
$\left\|\mathrm{Im}\left[\boldsymbol{C}_Q^{23}\boldsymbol{C}_{u_R}^{*23}\right]/f_a^2\right\| < \left(\frac{m_t^2}{m_a^2+m_t^2}\right)1\times10^{-14}$
$\left\|\mathrm{Im}\left[\boldsymbol{C}_Q^{13}\boldsymbol{C}_{d_R}^{*13}\right]/f_a^2\right\| < \left(\frac{m_b^2}{m_a^2+m_b^2}\right)3\times10^{-12}$
$\left\|\mathrm{Im}\left[\boldsymbol{C}_Q^{12}\boldsymbol{C}_{u_R}^{*12}\right]/f_a^2\right\| < \left(\frac{m_c^2}{m_a^2+m_c^2}\right)5\times10^{-11}$
$\left\|\mathrm{Im}\left[\boldsymbol{C}_Q^{23}\boldsymbol{C}_{d_R}^{*23}\right]/f_a^2\right\| < \left(\frac{m_b^2}{m_a^2+m_b^2}\right)6\times10^{-11}$
$\left\|\mathrm{Im}\left[\boldsymbol{C}_Q^{12}\boldsymbol{C}_{d_R}^{*12}\right]/f_a^2\right\| < \left(\frac{m_s^2}{m_a^2+m_s^2}\right)3\times10^{-7}$

$$\left|\frac{\mathrm{Im}[\boldsymbol{C}_Q^{13}\boldsymbol{C}_{u_R}^{*13}]}{f_a^2}\right|_{\bar{\theta}} \lesssim \left(\frac{m_t^2}{m_a^2+m_t^2}\right)2\times10^{-17}\ \mathrm{GeV}^{-2}. \quad (15)$$

Here and below, we conservatively assume $\log f_a^2/m_a^2 \sim 1$ and also disregard the running of the quark masses (although the bounds could become stronger by over an order of magnitude for $f_a/m_a > 10^2$; see Sec. D). Projections from future nEDM and pEDM measurements are expected to improve this bound by 3 orders of magnitude.

In Table I, we show the corresponding results for all the other combinations of couplings $|\mathrm{Im}[\boldsymbol{C}_Q^{ij}\boldsymbol{C}_{q_R}^{*ij}]/f_a^2|$. *All bounds in this paper consider one coupling combination at a time.* We have used the PDG values for the quark masses [51]. The same bounds are also represented with solid colors in Fig. 2 as a function of m_a. The region below $m_a = 1$ GeV appears shaded in gray—here and in all figures below—since it lies outside the validity of our approximations, and a proper treatment would require an alternative computation where the ALP is included in the chiral Lagrangian, similarly to Refs. [24,25]. For improved plot clarity, future projections are exclusively depicted for the most constrained coupling combination, $|\mathrm{Im}(\boldsymbol{C}_Q^{13}\boldsymbol{C}_{q_R}^{13})|$. However, it is important to note that all solid regions will be shifted downward by the same factor based on forthcoming nEDM and pEDM measurements.

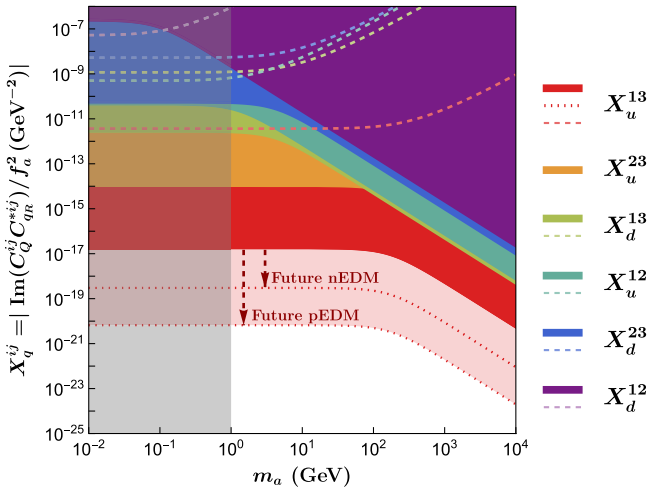

FIG. 2. *ALP case.* Bounds as a function of m_a. Upper bounds on $X_q^{ij} \equiv |\mathrm{Im}(\boldsymbol{C}_Q^{ij}\boldsymbol{C}_{q_R}^{ij})/f_a^2|$ from the $\bar{\theta}$ correction (solid regions) and from qEDMs and cEDMs (dashed lines). Future bounds stemming from nEDM and pEDM projections [52] are indicated for $\boldsymbol{X}_u^{13}$ with a red dotted line. For ALP masses near or below the QCD threshold ($m_a \lesssim 1$ GeV, shaded region), the results are outside the validity of our approximations; see text.

A. Comparison with quark EDM contributions

The Lagrangian in Eq. (1) also generates a contribution to the individual qEDMs $d_{u,d,s}$ and cEDMs $\tilde{d}_{u,d,s}$, which in turn contribute to the final nEDM value through Eq. (13). The corresponding Feynman diagram—see Fig. 3—has been previously computed [22,53], and for the up-quark EDM, it contributes as

$$\frac{d_u}{e} \equiv \frac{Q_u}{32\pi^2 f_a^2}\mathrm{Im}\left[\mathbf{C}_Q \boldsymbol{G} \mathbf{C}_{u_R}^\dagger\right]_{11}, \quad (16)$$

with $\boldsymbol{G} = \mathrm{diag}(G(x_u), G(x_c), G(x_t))$ and

$$G(x_k) \equiv m_a x_k^{3/2}\frac{\left(3-4x_k+x_k^2+2\log(x_k)\right)}{(x_k-1)^3} \sim \frac{m_k}{m_a^2}\mathtt{min}\left(m_a^2, 3m_k^2\right), \quad (17)$$

where $x_k \equiv m_k^2/m_a^2$, $Q_u = +2/3$ is the charge of the up quark in units of e, and the last expression captures the order of magnitude for either $m_a \ll m_k$ or $m_a \gg m_k$. An analogous expression holds for the ALP induced d_d. Also, the same Feynman diagram depicts the one-loop contribution to the quark cEDM $\tilde{d}_q$ by replacing the photon with a gluon, and its computation can be simply recast from that for the qEDM as $\tilde{d}_q = d_q/eQ_{u,d}$, where the g_s factor is customarily factored out in the definition, see Eq. (3).

The d_q and $\tilde{d}_q$ contributions to the nEDM are comparable, and again, the strongest bound corresponds to that involving the top quark in the loop,

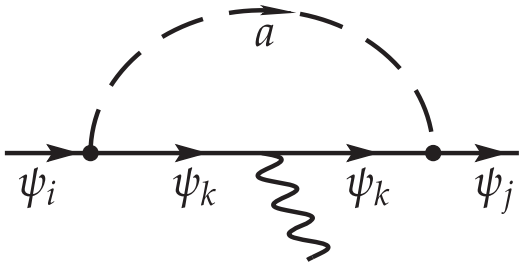

FIG. 3. ALP-induced one loop contribution to the fermion-photon vertex as considered in Ref. [22].

TABLE II. *ALP case.* Bounds from $\bar{\theta}$ contributions versus qEDM and cEDM bounds. Experimental bounds on $|\mathrm{Im}[\boldsymbol{C}_Q^{ij}\boldsymbol{C}_{q_R}^{*ij}]/f_a^2|$ for the particular case $m_a = 5$ GeV. The last column corresponds to the sum of the qEDM and cEDM contributions. The bounds can be extrapolated to other values of m_a using Eqs. (11) and (17), respectively.

Combination	$\bar{\theta}$ bounds (GeV^{-2})	qEDM & cEDM (GeV^{-2})
$\lvert\mathrm{Im}[\boldsymbol{C}_Q^{13}\boldsymbol{C}_{u_R}^{*13}]/f_a^2\rvert$	1.8×10^{-17}	3.7×10^{-12}
$\lvert\mathrm{Im}[\boldsymbol{C}_Q^{23}\boldsymbol{C}_{u_R}^{*23}]/f_a^2\rvert$	1.1×10^{-14}	8.3×10^{-8}
$\lvert\mathrm{Im}[\boldsymbol{C}_Q^{13}\boldsymbol{C}_{d_R}^{*13}]/f_a^2\rvert$	1.1×10^{-12}	1.9×10^{-9}
$\lvert\mathrm{Im}[\boldsymbol{C}_Q^{12}\boldsymbol{C}_{u_R}^{*12}]/f_a^2\rvert$	2.7×10^{-12}	2.3×10^{-9}
$\lvert\mathrm{Im}[\boldsymbol{C}_Q^{23}\boldsymbol{C}_{d_R}^{*23}]/f_a^2\rvert$	2.3×10^{-11}	8.7×10^{-9}
$\lvert\mathrm{Im}[\boldsymbol{C}_Q^{12}\boldsymbol{C}_{d_R}^{*12}]/f_a^2\rvert$	8.6×10^{-11}	1.2×10^{-5}

$$\left|\frac{\mathrm{Im}(\boldsymbol{C}_Q^{13}\boldsymbol{C}_{u_R}^{*13})}{f_a^2}\right|_{d_q,\tilde{d}_q} \lesssim 3.7 \times 10^{-12}\ \mathrm{GeV}^{-2}, \tag{18}$$

which is several orders of magnitude weaker than that obtained in Eq. (15) from $\bar{\theta}$.

Similarly, separate bounds on the other possible combinations of parameters can be obtained using Eqs. (13) and (17). As an example, in Table II, we compare the bounds for the CP-odd combinations $X_q^{ij} \equiv |\mathrm{Im}(\boldsymbol{C}_Q^{ij}\boldsymbol{C}_{q_R}^{ij})/f_a^2|$ stemming from the qEDM and cEDM with those resulting from our analysis of the $\bar{\theta}$ parameter for an ALP mass $m_a = 5$ GeV. Indirect contributions from the charm and bottom (c)qEDM, not included in Eq. (13), give bounds on $|\mathrm{Im}[\boldsymbol{C}_Q^{23}\boldsymbol{C}_{u_R}^{*23}]/f_a^2|$ [54,55]; Fig. 2 depicts, as a function of m_a, the bounds from $\bar{\theta}$ in solid regions and those from qEDM and cEDM with dashed lines. It is seen that, for $m_a \gtrsim 1$ GeV, the dominant bounds on X_q^{ij} arise from the ALP contribution to $\bar{\theta}$.

Complementary bounds on these parameters can be obtained from CP violation in $\Delta F = 2$ processes.[9] For example, from $K - \bar{K}$ mixing, one obtains [56]

$$\frac{1}{f_a^2}\left|\mathrm{Im}\left[\left(C_Q^{12} - C_{d_R}^{12}\right)^2\right]\right| \lesssim 10^{-13}\left(\frac{m_a}{5\ \mathrm{GeV}}\right)^2\ \mathrm{GeV}^{-2}. \tag{19}$$

This strong bound corresponds to a different direction in parameter space and has a different parametric dependence on m_a.

We have cross-checked our results by performing the computation in an alternative basis; see Sec. A. Indeed, the chirality-preserving ALP-fermion interactions in Eq. (1) can be traded for a specific combination of Yukawa-like operators in the so-called "chirality-flip basis" via a suitable field redefinition of the fields. As this is only a change of basis, the number of free parameters does not change.

V. GENERIC SCALAR WITH *CP*-ODD FERMIONIC INTERACTIONS

In this section, the previous analysis is extended to a theory of a singlet scalar ϕ with mass m_ϕ and coupled to SM fermions without imposing shift symmetry.

The most general CP-odd fermion-scalar interactions are described by a Lagrangian exhibiting Yukawa-like left-right interactions,

$$\mathcal{L} \supset \bar{u}_L v\left[i\boldsymbol{K}_u\frac{\phi}{\Lambda} + \boldsymbol{F}_u\frac{\phi^2}{\Lambda^2}\right]u_R + \bar{d}_L v\left[i\frac{\phi}{\Lambda}\boldsymbol{K}_d + \frac{\phi^2}{\Lambda^2}\boldsymbol{F}_d\right]d_R + \mathrm{H.c.} \tag{20}$$

where $\boldsymbol{K}_q$ and $\boldsymbol{F}_q$ are arbitrary 3×3 dimensionless coefficient matrices in flavor space, and Λ denotes the new physics scale. The dependence on the Higgs vacuum expectation value, $v = 246$ GeV, is a remnant of the couplings ancestry above the electroweak scale, which corresponds to Yukawa-like operators of mass dimension 5 ($\boldsymbol{K}_q$ terms) and 6 ($\boldsymbol{F}_q$ terms). The $\mathcal{O}(1/\Lambda^2)$ $\boldsymbol{F}_q$ terms have been included as this is required by the consistency of the EFT analysis at one loop. They contribute to $\bar{\theta}$ through the lower diagram in Fig. 4 at the same order as the first one (which presents two insertions of the coupling proportional to $\boldsymbol{K}_d/\Lambda$). Even considering only the $\boldsymbol{K}_q$ terms, this Lagrangian has more free parameters than that for the ALP in Eq. (1) (see also Appendix A). Those extra parameters

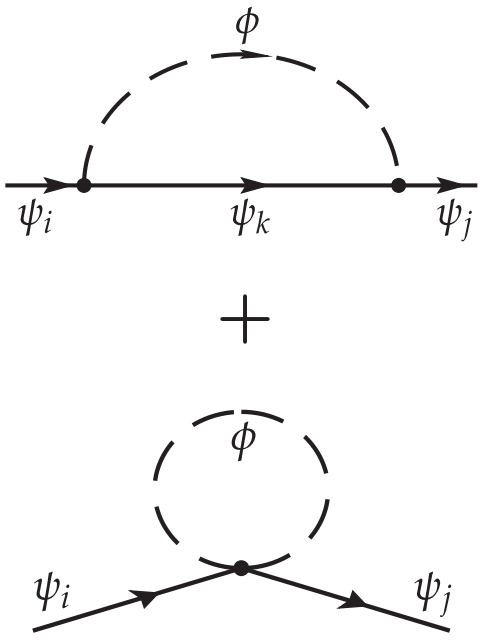

FIG. 4. Scalar exchange one-loop contribution to the quark masses.

[9]We thank Andreas Trautner and the referee for raising this issue.

include flavor-diagonal ones that can be complex, thus sourcing additional *CP*-violation effects, in contrast to the case of the ALP theory.

In the literature, it is also common to use the alternative notation

$$\bar{q}_L i v \frac{a}{f_a} \boldsymbol{K}_q q_R \equiv \frac{a}{f_a} v\left(\bar{q}\, \boldsymbol{y}_{qS} q + i \bar{q}\, \boldsymbol{y}_{qP} \gamma_5 q\right), \tag{21}$$

with

$$\boldsymbol{y}_{qS} \equiv i \frac{\boldsymbol{K}_q - \boldsymbol{K}_q^\dagger}{2}, \qquad \boldsymbol{y}_{qP} \equiv \frac{\boldsymbol{K}_q + \boldsymbol{K}_q^\dagger}{2}. \tag{22}$$

The contribution of the $\boldsymbol{K}_q$ and $\boldsymbol{F}_q$ parameters to $\bar{\theta}$ through its running reads:

$$\bar{\theta}(\mu_{\rm IR}) \simeq \bar{\theta}_0 + \frac{v^2}{16\pi^2\Lambda^2} \times \left(\sum_{i,k} \left[\frac{m_{u_k} \mathrm{Im}(\boldsymbol{K}_u^{ik} \boldsymbol{K}_u^{ki})}{m_{u_i}} - \frac{m_\phi^2 \mathrm{Im}(\boldsymbol{F}_u^{ik})}{v m_{u_i}} \right] \log \frac{\Lambda^2}{\mathtt{max}\left(m_\phi^2, m_{u_k}^2\right)} + \sum_{i,k} \left[\frac{m_{d_k} \mathrm{Im}(\boldsymbol{K}_d^{ik} \boldsymbol{K}_d^{ki})}{m_{d_i}} - \frac{m_\phi^2 \mathrm{Im}(\boldsymbol{F}_d^{ik})}{v m_{d_i}} \right] \log \frac{\Lambda^2}{\mathtt{max}\left(m_\phi^2, m_{d_k}^2\right)} \right). \tag{23}$$

In turn, their contribution to the up-quark EDM is given by

$$\frac{d_u}{e} \equiv \frac{Q_u}{32\pi^2} \frac{v^2}{\Lambda^2} \mathrm{Im}\left[\mathbf{K}_q \boldsymbol{G}' \mathbf{K}_q^\dagger\right]_{11}, \tag{24}$$

with $\boldsymbol{G}' = \mathrm{diag}(G'(x_u), G'(x_c), G'(x_t))$, where $x_k \equiv m_k^2/m_\phi^2$, and

$$G'(x_k) \equiv \frac{x_k^{1/2}}{m_\phi} \frac{(3 - 4x_k + x_k^2 + 2\log(x_k))}{(x_k - 1)^3},$$

and analogously for the other flavors and for the quark cEDMs [22].

Stringent restrictions on this enlarged $\{\boldsymbol{K}_q, \boldsymbol{F}_q\}$ parameter space follow from the nEDM experimental limit [20,57], with an impact comparable to that found in the previous sections for the *CP*-odd couplings of a generic ALP. Using again Eq. (13), the nEDM is seen to be sensitive to the combinations $W_q^{ij} \equiv |\mathrm{Im}(\boldsymbol{K}_q^{ij} \boldsymbol{K}_q^{ji})/\Lambda^2|$ and $V_q^{ii} \equiv |\mathrm{Im}(\boldsymbol{F}_q^{ii})/\Lambda^2|$. The corresponding bounds are displayed in Table III and depicted as a function of m_ϕ in Figs. 5 and 6. For most W_q^{ij}'s, the constraint imposed by their contribution to $\bar{\theta}$ dominates strongly over that from contributions to qEDMs and cEDMs. In addition, the contributions to $\bar{\theta}$ also provide a handle into several combinations of parameters—W_u^{33} and the V_q^{ii}'s—which do not contribute to neither the qEDMs nor the cEDMs.

Analogously to the ALP case in Eq. (19), complementary bounds for different directions in the parameter space of the general scalar can be obtained from *CP* violation in $\Delta F = 2$ processes such as meson mixing [56].

In summary, much as in the case of ALPS, the bounds obtained for a general scalar are several orders of magnitude stronger than those existing in the literature due to the impact of the $\bar{\theta}$ parameter. Furthermore, some new combinations of parameters have become accessible via the present $\bar{\theta}$ analysis.

TABLE III. *General scalar.* Bounds on $|\mathrm{Im}(\boldsymbol{K}_q^{ij} \boldsymbol{K}_q^{ji})/\Lambda^2|$ and $|\mathrm{Im}(\boldsymbol{F}_q^{ii})/\Lambda^2|$ stemming from their contribution to the nEDM. The bounds on $|\mathrm{Im}(\boldsymbol{K}_q^{ij} \boldsymbol{K}_q^{ji})/\Lambda^2|$ inferred from their contribution to $\bar{\theta}$ are independent of m_ϕ, while those stemming from the sum of qEDMs and cEDMs are evaluated for $m_\phi = 5$ GeV. The bounds that stem from the indirect effect of the charm and bottom (c)qEDMs are derived from [55].

Combination	$\bar{\theta}$-bounds (GeV^{-2})	qEDM & cEDM (GeV^{-2})
$\left\|\mathrm{Im}\left(\boldsymbol{K}_u^{13}\boldsymbol{K}_u^{31}\right)/\Lambda^2\right\|$	8.9×10^{-18}	9.0×10^{-13}
$\left\|\mathrm{Im}\left(\boldsymbol{K}_d^{13}\boldsymbol{K}_d^{31}\right)/\Lambda^2\right\|$	7.9×10^{-16}	2.8×10^{-13}
$\left\|\mathrm{Im}\left(\boldsymbol{K}_u^{12}\boldsymbol{K}_u^{21}\right)/\Lambda^2\right\|$	1.2×10^{-15}	3.1×10^{-14}
$\left\|\mathrm{Im}\left(\boldsymbol{K}_u^{23}\boldsymbol{K}_u^{32}\right)/\Lambda^2\right\|$	5.2×10^{-15}	2.1×10^{-8}
$\left\|\mathrm{Im}\left(\boldsymbol{K}_d^{23}\boldsymbol{K}_d^{32}\right)/\Lambda^2\right\|$	1.6×10^{-14}	1.3×10^{-12}
$\left\|\mathrm{Im}\left(\boldsymbol{K}_d^{12}\boldsymbol{K}_d^{21}\right)/\Lambda^2\right\|$	3.5×10^{-14}	8.2×10^{-13}
$\left\|\mathrm{Im}\left(\boldsymbol{K}_u^{11}\boldsymbol{K}_u^{11}\right)/\Lambda^2\right\|$	7.1×10^{-13}	2.2×10^{-12}
$\left\|\mathrm{Im}\left(\boldsymbol{K}_d^{11}\boldsymbol{K}_d^{11}\right)/\Lambda^2\right\|$	7.1×10^{-13}	8.7×10^{-12}
$\left\|\mathrm{Im}\left(\boldsymbol{K}_d^{22}\boldsymbol{K}_d^{22}\right)/\Lambda^2\right\|$	7.1×10^{-13}	3.8×10^{-12}
$\left\|\mathrm{Im}\left(\boldsymbol{K}_u^{22}\boldsymbol{K}_u^{22}\right)/\Lambda^2\right\|$	7.1×10^{-13}	7.0×10^{-10}
$\left\|\mathrm{Im}\left(\boldsymbol{K}_u^{33}\boldsymbol{K}_u^{33}\right)/\Lambda^2\right\|$	7.1×10^{-13}	⋯
$\left\|\mathrm{Im}\left(\boldsymbol{K}_d^{33}\boldsymbol{K}_d^{33}\right)/\Lambda^2\right\|$	7.1×10^{-13}	5.5×10^{-8}
$\left\|\mathrm{Im}\left(\boldsymbol{F}_u^{11}\right)/\Lambda^2\right\|$	1.5×10^{-14}	⋯
$\left\|\mathrm{Im}\left(\boldsymbol{F}_d^{11}\right)/\Lambda^2\right\|$	3.3×10^{-14}	⋯
$\left\|\mathrm{Im}\left(\boldsymbol{F}_d^{22}\right)/\Lambda^2\right\|$	6.5×10^{-13}	⋯
$\left\|\mathrm{Im}\left(\boldsymbol{F}_u^{22}\right)/\Lambda^2\right\|$	8.9×10^{-12}	⋯
$\left\|\mathrm{Im}\left(\boldsymbol{F}_d^{33}\right)/\Lambda^2\right\|$	2.9×10^{-11}	⋯
$\left\|\mathrm{Im}\left(\boldsymbol{F}_u^{33}\right)/\Lambda^2\right\|$	1.2×10^{-9}	⋯

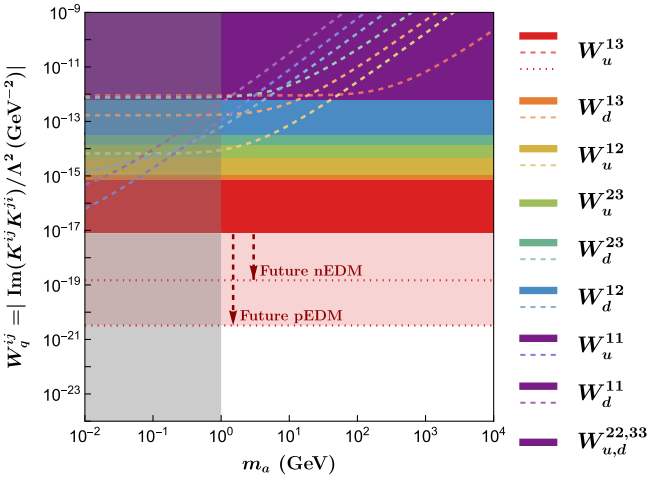

FIG. 5. *General scalar.* Upper bounds on $W_q^{ij} \equiv |\mathrm{Im}(\boldsymbol{K}_q^{ij}\boldsymbol{K}_q^{ji})/\Lambda^2|$ stemming from the contributions of $\bar{\theta}$ (solid regions) and from the sum of qEDMs and cEDMs (dashed lines) to the nEDM. The red dotted line shows the projected bounds on W_u^{13} from future nEDM and pEDM experiments [47,48]. The gray shaded area is as described in Fig. 2.

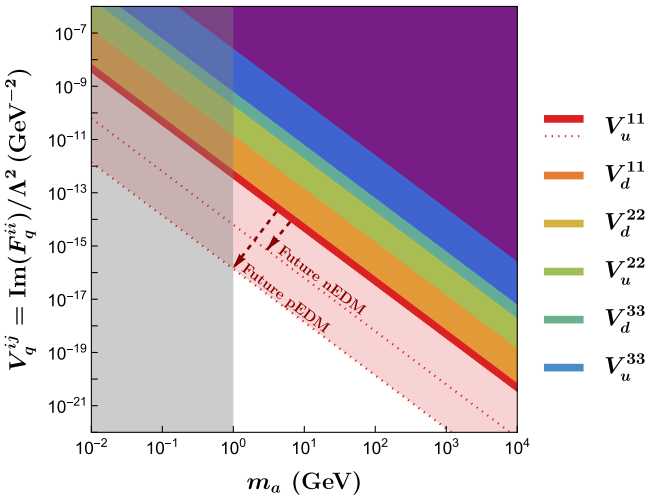

FIG. 6. *General scalar.* Upper bounds on $V_q^{ij} \equiv |\mathrm{Im}(F_q^{ij})/\Lambda^2|$ stemming from the contributions of $\bar{\theta}$ (solid regions) to the nEDM. The red dotted line shows the projected bounds on V_u^{11} from future nEDM and pEDM experiments [47,48]. The gray shaded area is as described in previous plots.

VI. DISCUSSION

In this work, we have computed the one-loop contribution to the $\bar{\theta}$ parameter of an ALP with *CP*-odd derivative couplings to fermions. Its impact on the nEDM is such that the bounds obtained on the *CP*-odd ALP-fermion couplings are many orders of magnitude stronger than those stemming from the contributions to up- and down-quark electric and chromo-electric dipole moments. The same conclusion applies to the *CP*-odd fermionic couplings of a generic scalar particle.

Finally, it is worth mentioning that the strong novel bounds found above, either for an ALP theory or for a general scalar, do not apply if those theories are extended by including in the Lagrangian—in addition to the ALP—an extra true QCD axion that solves the strong *CP* problem via a Peccei-Quinn mechanism. In that case, the QCD axion would absorb all contributions to $\bar{\theta}$ computed in this work. Still a nonzero induced $\bar{\theta}_{\mathrm{ind}}$ [45,58–60] would remain, leading to weaker but significant bounds on the studied couplings [22,24]. We expand on that case in Sec. C.

ACKNOWLEDGMENTS

We thank Jesús Bonilla and María Ramos for illuminating discussions in the early stages of this project. We thank Jonathan Kley for pointing us to the most updated estimation of the qEDM contributions to the nEDM. We also thank Luca di Luzio and Maxim Pospelov for clarifications on their work, as well as Ilaria Brivio, Zoltan Ligeti, Alessandro Valenti and Andreas Trautner for illuminating comments and advice. This project has received funding/support from the European Union's Horizon 2020 research and innovation programme under the Marie Sklodowska-Curie Grant Agreement No. 860881-HIDDeN and under the Marie Sklodowska-Curie Staff Exchange Grant Agreement No. 101086085-ASYMMETRY. The work of B. Gr. and P. Q. is supported in part by the U.S. Department of Energy Grant No. DE-SC0009919. The work of V. E. was supported by the Spanish Ministerio de Ciencia, Innovación y Universidades (MICIU) through the National Program FPI-Severo Ochoa (Grant No. PRE2020-094281). B. Ga. and V. E. acknowledge as well partial financial support from the Spanish Research Agency (Agencia Estatal de Investigación) through the Grant IFT Centro de Excelencia Severo Ochoa No. CEX2020-001007-S, Grants No. PID2019-108892RB-I00 and No. PID2022-137127NB-I00 funded by MCIN/AEI/10.13039/501100011033/FEDER, UE. B. Ga. and V. E. thank very much the Particle Physics group of the University of California, San Diego, where part of this work was carried out.

APPENDIX A: CHIRALITY-FLIP BASIS

As a double check and to facilitate the comparison of our results with the rest of the literature, we have also computed the ALP-fermion contribution to $\bar{\theta}$ in the chirality-flip basis. It is well known [33,61,62] that by applying the transformation

$$u_L \longrightarrow e^{i\frac{a}{f_a}\boldsymbol{C}_Q} u_L, \qquad d_L \longrightarrow e^{i\frac{a}{f_a}\boldsymbol{C}_Q} d_L, \tag{A1}$$

$$u_R \longrightarrow e^{i\frac{a}{f_a}\boldsymbol{C}_{u_R}} u_R, \qquad d_R \longrightarrow e^{i\frac{a}{f_a}\boldsymbol{C}_{d_R}} d_R \tag{A2}$$

to the Lagrangian in Eq. (1), one can trade the derivative ALP-fermionic interactions by Yukawa-like left-right interactions as described by

$$\mathcal{L} \supset \bar{u}_L v\left[i\frac{a}{f_a}\boldsymbol{K}_u + \frac{a^2}{f_a^2}\boldsymbol{F}_u\right]u_R + \bar{d}_L v\left[i\frac{a}{f_a}\boldsymbol{K}_d + \frac{a^2}{f_a^2}\boldsymbol{F}_d\right]d_R + \text{H.c.} + \ldots, \tag{A3}$$

where the $\boldsymbol{K}_q$ and $\boldsymbol{F}_q$ coefficient matrices are given by

$$\begin{aligned} v\boldsymbol{K}_q &\equiv \boldsymbol{C}_Q\boldsymbol{M}_q - \boldsymbol{M}_q\boldsymbol{C}_{q_R}, \\ 2v\boldsymbol{F}_q &\equiv 2\boldsymbol{C}_Q\boldsymbol{M}_q\boldsymbol{C}_{q_R} - \boldsymbol{C}_Q^2\boldsymbol{M}_q - \boldsymbol{M}_q\boldsymbol{C}_{q_R}^2, \end{aligned} \tag{A4}$$

and the ellipsis stands for higher order terms $\mathcal{O}(1/f_a^3)$.

The Lagrangian in Eq. (A3) is formally the same as that in Eq. (20) for a general scalar (with the replacement $\phi \to a$ and $\Lambda \to f_a$), but the relations in Eq. (A4) reduce its degrees of freedom. They ensure that it is shift symmetric under $a \to a + \text{constant}$ and equivalent to the ALP Lagrangian in Eq. (1).

In this chirality-flip basis, the two diagrams in Fig. 4 contribute to the one-loop corrections to the quark masses (in contrast with the derivative basis where only the first topology contributes). In particular, it is this second diagram that exhibits the quadratic divergence $\propto m_a^2$. It is straightforward to check that the result obtained in the derivative basis, Eq. (12), is recovered by substituting Eq. (A4) into Eq. (23).

APPENDIX B: NEDM ESTIMATES FROM QCD SUM RULES WITHOUT A PECCEI-QUINN SYMMETRY

Various methods, including naive dimensional analysis [63], chiral lagrangians [64,65], lattice simulations [43] and QCD sum rules [44,66], can be employed to obtain estimates of the nEDM and pEDM as a function of $\bar{\theta}$, d_q and $\tilde{d}_q$. Their corresponding results do not always agree with each other and present a large span of uncertainties.

Thoughout this paper, we will use the lattice result in Ref. [43] for the coefficients of the qEDMs in the nEDM and pEDM formulas,

$$\begin{aligned} d_n(d_q) &= -0.204(11)d_u + 0.784(28)d_d - 0.0028(17)d_s \\ d_p(d_q) &= +0.784(28)d_u - 0.204(11)d_d - 0.0028(17)d_s. \end{aligned} \tag{B1}$$

Note that the estimation in Ref. [22] has a typographical error as the numerical coefficients for d_u and d_d appear interchanged with respect to the lattice results in Ref. [43].

For the rest of the coefficients $d_n(\bar{\theta}, \tilde{d}_q)$, we will use the analytical formulas from QCD sum rule estimates in Ref. [46] for the nEDM. The formula for $d_p(\bar{\theta}, \tilde{d}_q)$ is obtained by interchanging $u \leftrightarrow d$ in $d_n(\bar{\theta}, \tilde{d}_q)$. The result reads

$$d_{n,p}(\bar{\theta}, \tilde{d}_q, d_q) = -c_0\frac{\langle\bar{q}q\rangle}{\lambda_N^2 m_{n,p}}\Theta_{n,p}(\bar{\theta}, \tilde{d}_q, d_q), \tag{B2}$$

where $c_0 = 1.8 \times 10^{-2}$ GeV^4 [46], $m_{n,p}$, respectively, denote the neutron and proton mass, the value of the chiral condensate will be taken from the recent computation in Ref. [67] $\langle\bar{q}q\rangle = -(0.272(5)\text{ GeV})^3$ and the low-energy constant $\lambda_N = -0.0436(131)$ GeV^3 will be taken from a lattice calculation [46]. The $\Theta_{n,p}$ functions are given by

$$\begin{aligned} \Theta_n(\bar{\theta}, \tilde{d}_q, d_q) &= \chi m_*\left[(4e_d - e_u)\left(\bar{\theta} - \frac{m_0^2}{2}\frac{\tilde{d}_s}{m_s}\right) + \frac{m_0^2}{2}(\tilde{d}_d - \tilde{d}_u)\left(\frac{4e_d}{m_u} + \frac{e_u}{m_d}\right) + \frac{m_0^2}{2}\left(\frac{4e_d}{m_s}\tilde{d}_d - \frac{e_u}{m_s}\tilde{d}_u\right)\right] \\ &\quad + \left(\kappa - \frac{1}{2}\xi\right)(4e_d\tilde{d}_d - e_u\tilde{d}_u) + (4d_d - d_u), \\ \Theta_p(\bar{\theta}, \tilde{d}_q, d_q) &= \chi m_*\left[(4e_u - e_d)\left(\bar{\theta} - \frac{m_0^2}{2}\frac{\tilde{d}_s}{m_s}\right) + \frac{m_0^2}{2}(\tilde{d}_u - \tilde{d}_d)\left(\frac{4e_u}{m_d} + \frac{e_d}{m_u}\right) + \frac{m_0^2}{2}\left(\frac{4e_u}{m_s}\tilde{d}_u - \frac{e_d}{m_s}\tilde{d}_d\right)\right] \\ &\quad + \left(\kappa - \frac{1}{2}\xi\right)(4e_u\tilde{d}_u - e_d\tilde{d}_d) + (4d_u - d_d). \end{aligned} \tag{B3}$$

where $m_* \equiv (1/m_u + 1/m_s + 1/m_s)^{-1}$, e_u and e_d denote the electromagnetic charges of the up and down quarks ($e_u = +2/3e$, $e_d = -1/3e$) and the parameters $m_0^2 = 0.8(2)$ GeV^2, $\kappa = -0.34(10)$, $\chi = -5.7(6)$ GeV^{-2} [68,69] and $\xi = -0.74(20)$ [70,71] are as defined in Eqs. (48)–(50) in Ref. [46]. Substituting these input parameters in Eqs. (B2) and (B3), we finally obtain:

$$\begin{aligned} d_n(\bar{\theta}, \tilde{d}_q, d_q) &= 0.6(3) \times 10^{-16}\bar{\theta}\,[e\cdot\text{cm}] - 0.2(1)d_u + 0.8(4)d_d - 0.0028(17)d_s \\ &\quad - 0.32(16)e\tilde{d}_u + 0.32(16)e\tilde{d}_d - 0.014(7)e\tilde{d}_s, \end{aligned} \tag{B4}$$

$$\begin{aligned} d_p(\bar{\theta}, \tilde{d}_q, d_q) &= -1.0(5) \times 10^{-16}\bar{\theta}\,[e\cdot\text{cm}] + 0.8(4)d_u - 0.2(1)d_d - 0.0028(17)d_s \\ &\quad - 0.26(13)e\tilde{d}_u + 0.28(14)e\tilde{d}_d + 0.02(1)e\tilde{d}_s. \end{aligned} \tag{B5}$$

Note that the coefficients of the qEDMs predicted from these QCD sum rules, with the updated the input values we use, are in good agreement with the lattice QCD result in Eq. (B1). The difference between our numerical results in Eqs. (B4) and (B5) and those in [46] result solely because we use an updated value for the quark condensate. Note that the apparent discrepancy in the powers of m_n in Eq. (B2) with respect to the expression in Ref. [72] results from the fact that the definition of the c_0 coefficient in Ref. [46] (and our results) differs by a factor of m_n^4 with respect to that in Ref. [72].

APPENDIX C: NEDM ESTIMATES IN THE PRESENCE OF A PECCEI-QUINN SYMMETRY

The presence of a Peccei-Quinn symmetry (with its corresponding QCD axion) modifies the nEDM estimates in Eq. (13). Firstly, the vev of the QCD axion will cancel the direct $\bar{\theta}$ dependence in the first term of Eq. (13). Secondly, the presence of explicit CP violation, e.g., via dipole moment couplings, shifts the minimum of the QCD axion potential away from the CP-conserving minimum, generating an induced $\bar{\theta}_{\rm ind}$ [45,58–60]. Indeed, for a chiral CP-odd theory such as that under consideration in Eq. (1), the Vafa-Witten [73] theorem does not apply and therefore cannot guarantee that the minimum of the axion sits exactly at the CP-conserving minimum. The value of $\bar{\theta}_{\rm ind}$ is dominated by the cEDM [60],

$$\bar{\theta}_{\rm ind} = \frac{m_0^2}{2} \sum_{q=u,d,s} \frac{\tilde{d}_q}{m_q}, \tag{C1}$$

where our sign convention for m_0^2 is that of [74]. Taking this induced $\bar{\theta}_{\rm ind}$ into account results into a modification of the coefficients in Eqs. (13) and (14), which now read [44,49]

$$\begin{aligned} d_n^{\rm PQ} = & -0.204(11) d_u + 0.784(28) d_d \\ & - 0.31(15) e\tilde{d}_u + 0.62(31) e\tilde{d}_d, \end{aligned} \tag{C2}$$

$$\begin{aligned} d_p^{\rm PQ} = & \, 0.784(28) d_u - 0.204(11) d_d \\ & - 1.21(60) e\tilde{d}_u - 0.15(7) e\tilde{d}_{.d} \end{aligned} \tag{C3}$$

This result was obtained by substituting, in the estimation of Eq. (13), $\bar{\theta}$ by the expression for $\bar{\theta}_{\rm ind}$ in Eq. (C1); i.e., $d_{n,p}^{\rm PQ}(d_{u,d}, \tilde{d}_{u,d}) = d_{n,p}(\bar{\theta} = \bar{\theta}_{\rm ind}, d_{u,d}, \tilde{d}_{u,d})$. It differs from the result in Ref. [44] because we are using a more refined estimation of $d_{n,p}(\bar{\theta})$ [65]. Note that in these two equations, the dependence on the qEDMs did not suffer any modification with respect to the estimation without PQ symmetry in Eqs. (13) and (14) since the induced $\bar{\theta}_{\rm ind}$ due to the existence of the qEDM is negligible [60], while the impact on the cEDMs is significant as earlier explained.

TABLE IV. *ALP case.* Comparison of bounds w/o the presence of a PQ symmetry. All bounds are in units of GeV^{-2}, and $m_a = 5$ GeV has been assumed for illustration.

Combination	With PQ (GeV^{-2})	Without PQ (GeV^{-2})
$\lvert \mathrm{Im}(\boldsymbol{C}_Q^{13}\boldsymbol{C}_{u_R}^{13})/f_a^2 \rvert$	3.7×10^{-12}	3.7×10^{-12}
$\lvert \mathrm{Im}(\boldsymbol{C}_Q^{13}\boldsymbol{C}_{d_R}^{13})/f_a^2 \rvert$	1.9×10^{-9}	3.2×10^{-9}
$\lvert \mathrm{Im}(\boldsymbol{C}_Q^{12}\boldsymbol{C}_{u_R}^{12})/f_a^2 \rvert$	2.3×10^{-9}	2.4×10^{-9}
$\lvert \mathrm{Im}(\boldsymbol{C}_Q^{23}\boldsymbol{C}_{d_R}^{23})/f_a^2 \rvert$	8.7×10^{-9}	1.2×10^{-7}
$\lvert \mathrm{Im}(\boldsymbol{C}_Q^{12}\boldsymbol{C}_{d_R}^{12})/f_a^2 \rvert$	1.2×10^{-5}	1.9×10^{-6}

TABLE V. *General scalar.* Comparison of bounds w/o the presence of a PQ symmetry through the (c)qEDMs. All bounds are in units of GeV^{-2}, and for $m_\phi = 5$ GeV.

Combination	With PQ (GeV^{-2})	Without PQ (GeV^{-2})
$\lvert \mathrm{Im}(\boldsymbol{K}_u^{13}\boldsymbol{K}_u^{31})/\Lambda^2 \rvert$	9.0×10^{-7}	9.2×10^{-7}
$\lvert \mathrm{Im}(\boldsymbol{K}_d^{13}\boldsymbol{K}_d^{31})/\Lambda^2 \rvert$	2.8×10^{-7}	4.6×10^{-8}
$\lvert \mathrm{Im}(\boldsymbol{K}_u^{12}\boldsymbol{K}_u^{21})/\Lambda^2 \rvert$	3.1×10^{-8}	3.1×10^{-8}
$\lvert \mathrm{Im}(\boldsymbol{K}_d^{23}\boldsymbol{K}_d^{23})/\Lambda^2 \rvert$	1.3×10^{-6}	1.8×10^{-5}
$\lvert \mathrm{Im}(\boldsymbol{K}_d^{12}\boldsymbol{K}_d^{21})/\Lambda^2 \rvert$	8.2×10^{-7}	1.4×10^{-7}
$\lvert \mathrm{Im}(\boldsymbol{K}_d^{22}\boldsymbol{K}_d^{22})/\Lambda^2 \rvert$	3.8×10^{-6}	5.3×10^{-5}
$\lvert \mathrm{Im}(\boldsymbol{K}_u^{11}\boldsymbol{K}_u^{11})/\Lambda^2 \rvert$	2.2×10^{-6}	2.2×10^{-6}
$\lvert \mathrm{Im}(\boldsymbol{K}_d^{11}\boldsymbol{K}_d^{11})/\Lambda^2 \rvert$	8.7×10^{-6}	1.4×10^{-6}

The resulting bounds on ALP-fermion CP-odd couplings are shown in Table IV for the case of an ALP with derivative couplings and in Table V for the case of a general scalar. In the latter case, no bounds result on the $\lvert \mathrm{Im}(\boldsymbol{F}_q^{ii})/\Lambda^2 \rvert$ coefficients, as their contribution is completely reabsorbed away by the Peccei-Quinn symmetry.

APPENDIX D: LEADING LOGS IN THE QUARK MASS RUNNING

Consider integration of Eq. (10) retaining dependence on the QCD coupling, α_s, so that the effect of running masses is retained. We neglect electroweak interactions since their effect is much smaller. To incorporate these effects, we solve Eq. (10) making use of the explicit derivative

$$\mu \frac{d}{d\mu} = \mu \frac{\partial}{\partial \mu} + \beta(g_s) \frac{\partial}{\partial g_s} + \sum_q m_q \gamma_m(g_s) \frac{\partial}{\partial m_q} \tag{D1}$$

and the observation that the couplings $\mathbf{C}_{Q,u_R,d_R}$ have vanishing anomalous dimensions because the corresponding operators in the Lagrangian of Eq. (1) are partially conserved currents in QCD. Denoting by $\bar{g}$ and $\bar{m}$ the running coupling and quark mass in QCD, that is, the solutions to

$$\mu\frac{d\bar{g}}{d\mu}=\beta(\bar{g}) \quad \text{and} \quad \mu\frac{d\bar{m}}{d\mu}=\gamma_m(\bar{g})\bar{m},$$

integration of Eq. (10) including the full μ-derivative of Eq. (D1) is equivalent to using only the $\mu\partial\bar{\theta}/\partial\mu$ on the left-hand side and substituting running couplings for the couplings on the right-hand side.

Leading-log resummation is achieved using one-loop running couplings. Using

$$\beta(g)=-b_0\frac{g^3}{16\pi^2} \quad \text{and} \quad \gamma_m(g)=a_m\frac{g^2}{16\pi^2}$$

with $b_0=11-2n_f/3$ and $a_m=-8$, the running couplings $\bar{\alpha}_s(\mu)$ are

$$\frac{1}{\bar{\alpha}_s(\mu)}-\frac{1}{\bar{\alpha}_s(\mu')}=\frac{b_0}{2\pi}\ln(\mu/\mu'), \tag{D2}$$

and

$$\bar{m}(\mu)=\bar{m}(\mu')\left(\frac{\bar{\alpha}_s(\mu)}{\bar{\alpha}_s(\mu')}\right)^{-a_m/2b_0}. \tag{D3}$$

Notice that the running of the factor of $\mathbf{M}^{-1}$ on the right-hand side on Eq. (10) cancels with the explicit overall mass factor in $\mathcal{L}$ of Eq. (11). What remains is an integral over $m_a^2+m_q^2$. The first of these is μ independent so that integration simply gives a logarithm of the ratio of scales, as in Eq. (12). For the second term, one needs

$$\int_{\mu'}^{\mu}\frac{d\mu}{\mu}\bar{m}^2=\int_{g'}^{g}\frac{d\bar{g}}{\beta(\bar{g})}\bar{m}(\bar{g})^2=-\frac{16\pi^2}{b_0}\bar{m}^2(\mu')\int_{g'}^{g}\frac{d\bar{g}}{\bar{g}^3}\left(\frac{g'}{\bar{g}}\right)^{2a_m/b_0}=\frac{8\pi^2}{b_0(1+a_m/b_0)}\left(\frac{\bar{m}^2(\mu)}{\bar{g}^2(\mu)}-\frac{\bar{m}^2(\mu')}{\bar{g}^2(\mu')}\right).$$

In the limit of vanishing coupling, $g\to 0$ this gives $m^2\ln(\mu/\mu_0)$, reproducing the explicit log in Eq. (12). Accordingly, one should use

$$\hat{m}_{q_k}^2\log(\mu_0^2/\mu_1^2)=\frac{4\pi}{b_0(1+a_m/b_0)}\left(\frac{\bar{m}^2(\mu_0)}{\bar{\alpha}_s(\mu_0)}-\frac{\bar{m}^2(\mu_1)}{\bar{\alpha}_s(\mu_1)}\right), \tag{D4}$$

with $\mu_0=f_a$ and $\mu_1=\max(m_a^2,m_{d_k}^2)$ in Eq. (12).

A couple of remarks are in order. First, when computing the ratios $m_{u_k}/m_{u_i}=\bar{m}_{u_k}(\mu)/\bar{m}_{u_i}(\mu)$ and $m_{d_k}/m_{d_i}=\bar{m}_{d_k}(\mu)/\bar{m}_{d_i}(\mu)$ at a common renormalization scale μ, the running of the mass and coupling constant may change as they cross through thresholds. For example, for the $m_{u_k}/m_{u_i}=m_t/m_u$ case, one writes the ratio in terms of $\bar{m}_t(m_t)$ and $\bar{m}_u(\mu_{\rm IR})$ with $\mu_{\rm IR}=2$ GeV, the values at the scales where they are often reported, as

$$\frac{m_t}{m_u}=\left(\frac{\bar{\alpha}_s^{(5)}(m_t)}{\bar{\alpha}_s^{(5)}(m_b)}\right)^{\frac{12}{23}}\left(\frac{\bar{\alpha}_s^{(4)}(m_b)}{\bar{\alpha}_s^{(4)}(\mu_{\rm IR})}\right)^{\frac{12}{25}}\frac{\bar{m}_t(m_t)}{\bar{m}_u(\mu_{\rm IR})},$$

where $\bar{\alpha}_s^{(n_f)}(\mu)$ is the running coupling of Eq. (D2) computed with n_f active quark flavors. And second, similarly, the effective mass in Eq. (D4) accounts for threshold effects additively. For example, if $m_a<m_b$, one should use

$$\hat{m}_b^2\log(\mu_0^2/m_b^2)=4\pi\bar{m}_b^2(m_b)\left[\left(\frac{\bar{\alpha}_s^{(5)}(m_t)}{\bar{\alpha}_s^{(5)}(m_b)}\right)^{\frac{24}{23}}\left(\frac{1}{\bar{\alpha}_s^{(6)}(m_t)}-\frac{1}{\bar{\alpha}_s^{(6)}(\mu_0)}\left(\frac{\bar{\alpha}_s^{(6)}(\mu_0)}{\bar{\alpha}_s^{(6)}(m_t)}\right)^{\frac{24}{21}}\right)\right.$$
$$\left.+3\left(\frac{1}{\bar{\alpha}_s^{(5)}(m_b)}-\frac{1}{\bar{\alpha}_s^{(5)}(m_t)}\left(\frac{\alpha_s^{(5)}(m_t)}{\alpha_s^{(5)}(m_b)}\right)^{\frac{24}{23}}\right)\right]. \tag{D5}$$

To get a sense of the magnitude of the leading log (LL) resummation, we take $m_a<m_t$ and $f_a=10^8$ GeV, which would be the minimum required from our conservative bounds in Table I for $|\mathrm{Im}[\boldsymbol{C}_Q^{13}\boldsymbol{C}_{u_R}^{*13}]|\sim 10^{-2}$. Then we use, naively, $\hat{m}_q=\bar{m}_q(m_q)$ and then compare both sides of Eq. (D4) and of Eq. (D5). Using $\bar{\alpha}_s^{(5)}(M_z)=0.12$, $m_t=175$ GeV, $m_b=4.2$ GeV, we obtain that the naive log overestimates the LL by factors of 1.8 and 2.8 in Eqs. (D4) and (D5), respectively. It is a curious coincidence that the running of the up quark from 1.0 GeV to m_t required to compute the factor $m_t(m_t)/m_u(m_t)$ in Eq. (12) is 1.8, exactly compensating for the LL resummation:

$$\frac{\bar{m}_t(m_t)}{\bar{m}_u(1\ \text{GeV})}\bar{m}_t^2(m_t)\approx\frac{\bar{m}_t(m_t)}{\bar{m}_u(m_t)}\hat{m}_t^2.$$

This coincidence is not generic; the running of the d or s quark masses from 1.0 GeV to m_b gives an enhancement of 1.3 to the ratio $m_b/m_{d,s}$, so the overall LL resummation effect is a a factor of 2.1 suppression.

We hasten to remind the reader that the bounds on couplings in Sec. IV use, conservatively, $\hat{m}_q^2 \log(f_a^2/\mu_1^2) \to m_q^2$, with $m_q = \bar{m}_q(m_q)$ for $q = t$, b, c and $\bar{m}_q(1\ \mathrm{GeV})$ for $q = u$, d, s. For the parameters chosen in the examples above, the neglected logarithmic factor is ∼20. It goes without saying that including this rather large logarithmic factor results in stronger bounds than the ones we obtained.

[1] R. D. Peccei and H. R. Quinn, *CP* conservation in the presence of instantons, Phys. Rev. Lett. **38**, 1440 (1977).
[2] R. D. Peccei and H. R. Quinn, Constraints imposed by *CP* conservation in the presence of instantons, Phys. Rev. D **16**, 1791 (1977).
[3] S. Weinberg, A new light boson?, Phys. Rev. Lett. **40**, 223 (1978).
[4] F. Wilczek, Problem of strong p and t invariance in the presence of instantons, Phys. Rev. Lett. **40**, 279 (1978).
[5] N. Arkani-Hamed and Y. Grossman, Light active and sterile neutrinos from compositeness, Phys. Lett. B **459**, 179 (1999).
[6] K. R. Dienes, E. Dudas, and T. Gherghetta, Invisible axions and large radius compactifications, Phys. Rev. D **62**, 105023 (2000).
[7] S. Chang, S. Tazawa, and M. Yamaguchi, Axion model in extra dimensions with TeV scale gravity, Phys. Rev. D **61**, 084005 (2000).
[8] L. Di Lella, A. Pilaftsis, G. Raffelt, and K. Zioutas, Search for solar Kaluza-Klein axions in theories of low scale quantum gravity, Phys. Rev. D **62**, 125011 (2000).
[9] A. Davidson and K. C. Wali, Minimal flavor unification via multigenerational Peccei-Quinn symmetry, Phys. Rev. Lett. **48**, 11 (1982).
[10] F. Wilczek, Axions and family symmetry breaking, Phys. Rev. Lett. **49**, 1549 (1982).
[11] Y. Ema, K. Hamaguchi, T. Moroi, and K. Nakayama, Flaxion: A minimal extension to solve puzzles in the standard model, J. High Energy Phys. 01 (2017) 096.
[12] L. Calibbi, F. Goertz, D. Redigolo, R. Ziegler, and J. Zupan, Minimal axion model from flavor, Phys. Rev. D **95**, 095009 (2017).
[13] L. F. Abbott and P. Sikivie, A cosmological bound on the invisible axion, Phys. Lett. **120B**, 133 (1983).
[14] M. Dine and W. Fischler, The not so harmless axion, Phys. Lett. **120B**, 137 (1983).
[15] J. Preskill, M. B. Wise, and F. Wilczek, Cosmology of the invisible axion, Phys. Lett. **120B**, 127 (1983).
[16] G. B. Gelmini and M. Roncadelli, Left-handed neutrino mass scale and spontaneously broken lepton number, Phys. Lett. **99B**, 411 (1981).
[17] M. Cicoli, axionlike particles from string compactifications, in *Proceedings, 9th Patras Workshop on Axions, WIMPs and WISPs (AXION-WIMP 2013): Mainz, Germany, 2013* (2013), pp. 235–242, 10.3204/DESY-PROC-2013-04/cicoli_michele.
[18] M. B. Gavela, A. Le Yaouanc, L. Oliver *et al.*, *CP* violation induced by Penguin diagrams and the neutron electric dipole moment, Phys. Lett. **109B**, 215 (1982).
[19] I. B. Khriplovich and A. R. Zhitnitsky, What is the value of the neutron electric dipole moment in the Kobayashi-Maskawa model?, Phys. Lett. **109B**, 490 (1982).
[20] C. Abel *et al.*, Measurement of the permanent electric dipole moment of the neutron, Phys. Rev. Lett. **124**, 081803 (2020).
[21] J. M. Pendlebury *et al.*, Revised experimental upper limit on the electric dipole moment of the neutron, Phys. Rev. D **92**, 092003 (2015).
[22] L. Di Luzio, R. Gröber, and P. Paradisi, Hunting for *CP*-violating axionlike particle interactions, Phys. Rev. D **104**, 095027 (2021).
[23] C. A. J. O'Hare and E. Vitagliano, Cornering the axion with *CP*-violating interactions, Phys. Rev. D **102**, 115026 (2020).
[24] W. Dekens, J. de Vries, and S. Shain, *CP*-violating axion interactions in effective field theory, J. High Energy Phys. 07 (2022) 014.
[25] L. Di Luzio, G. Levati, and P. Paradisi, The chiral Lagrangian of *CP*-violating axionlike particles, J. High Energy Phys. 02 (2024) 020.
[26] V. Plakkot, W. Dekens, J. de Vries, and S. Shaina, *CP*-violating axion interactions II: Axions as dark matter, J. High Energy Phys. 11 (2023) 012.
[27] Q. Bonnefoy, C. Grojean, and J. Kley, Shift-invariant orders of an axionlike particle, Phys. Rev. Lett. **130**, 111803 (2023).
[28] C. Grojean, J. Kley, and C.-Y. Yao, Hilbert series for ALP EFTs, J. High Energy Phys. 11 (2023) 196.
[29] M. Bauer, M. Neubert, S. Renner, M. Schnubel, and A. Thamm, Flavor probes of axionlike particles, J. High Energy Phys. 09 (2022) 056.
[30] L. Di Luzio, H. Gisbert, G. Levati *et al.*, *CP*-violating axions: A theory review, arXiv:2312.17310.
[31] A. Valenti and L. Vecchi, Perturbative running of the topological angles, J. High Energy Phys. 01 (2023) 131.
[32] T. Banno, J. Hisano, T. Kitahara, and N. Osamura, Closer look at the matching condition for radiative QCD θ parameter, J. High Energy Phys. 02 (2024) 195.
[33] H. Georgi, D. B. Kaplan, and L. Randall, Manifesting the invisible axion at low-energies, Phys. Lett. **169B**, 73 (1986).
[34] I. Brivio, M. B. Gavela, L. Merlo, K. Mimasu, J. M. No, R. del Rey, and V. Sanz, ALPs effective field theory and collider signatures, Eur. Phys. J. C **77**, 572 (2017).

[35] M. B. Gavela, R. Houtz, P. Quilez, R. del Rey, and O. Sumensari, Flavor constraints on electroweak ALP couplings, Eur. Phys. J. C **79**, 369 (2019).

[36] S. Weinberg, Goldstone bosons as fractional cosmic neutrinos, Phys. Rev. Lett. **110**, 241301 (2013).

[37] M. Bauer, G. Rostagni, and J. Spinner, Axion-Higgs portal, Phys. Rev. D **107**, 015007 (2023).

[38] J. R. Ellis and M. K. Gaillard, Strong and weak *CP* violation, Nucl. Phys. **B150**, 141 (1979).

[39] A. E. Nelson, Naturally weak *CP* violation, Phys. Lett. **136B**, 387 (1984).

[40] S. M. Barr, A natural class of non-Peccei-Quinn models, Phys. Rev. D **30**, 1805 (1984).

[41] M. Ahmed, R. Alarcon, A. Aleksandrova *et al.*, A new cryogenic apparatus to search for the neutron electric dipole moment, J. Instrum. **14**, P11017 (2019).

[42] J. Kley, T. Theil, E. Venturini, and A. Weiler, Electric dipole moments at one-loop in the dimension-6 SMEFT, Eur. Phys. J. C **82**, 926 (2022).

[43] R. Gupta, B. Yoon, T. Bhattacharya, V. Cirigliano, Y.-C. Jang, and H.-W. Lin, Flavor diagonal tensor charges of the nucleon from $(2 + 1 + 1)$-flavor lattice QCD, Phys. Rev. D **98**, 091501 (2018).

[44] M. Pospelov and A. Ritz, Electric dipole moments as probes of new physics, Ann. Phys. (Amsterdam) **318**, 119 (2005).

[45] M. Pospelov and A. Ritz, Neutron EDM from electric and chromoelectric dipole moments of quarks, Phys. Rev. D **63**, 073015 (2001).

[46] J. Hisano, K. Tsumura, and M. J. S. Yang, QCD corrections to neutron electric dipole moment from dimension-six four-quark operators, Phys. Lett. B **713**, 473 (2012).

[47] J. Alexander *et al.*, The storage ring proton EDM experiment, arXiv:2205.00830.

[48] S. N. Balashov, K. Green, M. G. D. van der Grinten *et al.*, A proposal for a cryogenic experiment to measure the neutron electric dipole moment (nEDM), arXiv:0709.2428.

[49] V. Cirigliano, A. Crivellin, W. Dekens, J. de Vries, M. Hoferichter, and E. Mereghetti, *CP* violation in Higgs-gauge interactions: From tabletop experiments to the LHC, Phys. Rev. Lett. **123**, 051801 (2019).

[50] B. Graner, Y. Chen, E. G. Lindahl, and B. R. Heckel, Reduced limit on the permanent electric dipole moment of ^{199}Hg, Phys. Rev. Lett. **116**, 161601 (2016).

[51] R. L. Workman *et al.* (Particle Data Group Collaboration), Review of particle physics, Prog. Theor. Exp. Phys. **2022**, 083C01 (2022).

[52] R. K. Ellis *et al.*, Physics briefing book: Input for the European strategy for particle physics update 2020, arXiv:1910.11775.

[53] S. Das Bakshi, J. Machado-Rodríguez, and M. Ramos, Running beyond ALPs: Shift-breaking and *CP*-violating effects, J. High Energy Phys. 11 (2023) 133.

[54] H. Gisbert and J. Ruiz Vidal, Improved bounds on heavy quark electric dipole moments, Phys. Rev. D **101**, 115010 (2020).

[55] Y. Ema, T. Gao, and M. Pospelov, Improved indirect limits on charm and bottom quark EDMs, J. High Energy Phys. 07 (2022) 106.

[56] M. Bona *et al.* (UTfit Collaboration), Model-independent constraints on $\Delta F = 2$ operators and the scale of new physics, J. High Energy Phys. 03 (2008) 049.

[57] J. M. Pendlebury *et al.*, Revised experimental upper limit on the electric dipole moment of the neutron, Phys. Rev. D **92**, 092003 (2015).

[58] I. I. Y. Bigi and N. G. Uraltsev, Effective gluon operators and the dipole moment of the neutron, Sov. Phys. JETP **73**, 198 (1991).

[59] M. Pospelov and A. Ritz, Theta induced electric dipole moment of the neutron via QCD sum rules, Phys. Rev. Lett. **83**, 2526 (1999).

[60] M. Pospelov, *CP* odd interaction of axion with matter, Phys. Rev. D **58**, 097703 (1998).

[61] M. Chala, G. Guedes, M. Ramos, and J. Santiago, Running in the ALPs, Eur. Phys. J. C **81**, 181 (2021).

[62] J. Bonilla, I. Brivio, M. B. Gavela, and V. Sanz, One-loop corrections to ALP couplings, J. High Energy Phys. 11 (2021) 168.

[63] A. Manohar and H. Georgi, Chiral quarks and the non-relativistic quark model, Nucl. Phys. **B234**, 189 (1984).

[64] R. J. Crewther, P. Di Vecchia, G. Veneziano, and E. Witten, Chiral estimate of the electric dipole moment of the neutron in quantum chromodynamics, Phys. Lett. **88B**, 123 (1979); **91B**, 487(E) (1980).

[65] F.-K. Guo and U.-G. Meissner, Baryon electric dipole moments from strong *CP* violation, J. High Energy Phys. 12 (2012) 097.

[66] M. A. Shifman, A. I. Vainshtein, and V. I. Zakharov, QCD and resonance physics. Theoretical foundations, Nucl. Phys. **B147**, 385 (1979).

[67] P. Gubler and D. Satow, Recent progress in QCD condensate evaluations and sum rules, Prog. Part. Nucl. Phys. **106**, 1 (2019).

[68] V. M. Belyaev and B. L. Ioffe, Determination of baryon and baryonic resonance masses from QCD sum rules. 1. Non-strange baryons, Sov. Phys. JETP **56**, 493 (1982).

[69] B. L. Ioffe and A. V. Smilga, Nucleon magnetic moments and magnetic properties of vacuum in QCD, Nucl. Phys. **B232**, 109 (1984).

[70] V. M. Khatsymovsky, On the experimental limits on the *CP* odd three gluon interaction, Sov. J. Nucl. Phys. **53**, 343 (1991).

[71] I. I. Kogan and D. Wyler, A Sum rule calculation of the neutron electric dipole moment from a quark chromoelectric dipole coupling, Phys. Lett. B **274**, 100 (1992).

[72] J. Hisano, D. Kobayashi, W. Kuramoto, and T. Kuwahara, Nucleon electric dipole moments in high-scale supersymmetric models, J. High Energy Phys. 11 (2015) 085.

[73] C. Vafa and E. Witten, Restrictions on symmetry breaking in vector-like gauge theories, Nucl. Phys. **B234**, 173 (1984).

[74] V. M. Belyaev and B. L. Ioffe, Determination of baryon and baryonic resonance masses from QCD sum rules. 1. Non-strange baryons, Sov. Phys. JETP **56**, 493 (1982).